JOURNAL OF MATERIALS SCIENCE **34** (1999) 925–931

Production and characterization of nanosized Cu/O/SiC composite particles in a thermal r.f. plasma reactor

P. BUCHNER[1], D. LÜTZENKIRCHEN-HECHT[2], H.-H. STREHBLOW[3], J. UHLENBUSCH[1]
[1] *Institut für Laser- und Plasmaphysik,* [2] *Institut für Angewandte Physik,* [3] *Institut für Physikalische Chemie und Elektrochemie, Heinrich-Heine-Universität Düsseldorf, Universitätsstr. 1, 40225 Düsseldorf, Germany*
E-mail: uhlenb@uni-duesseldorf.de

An inductively coupled thermal plasma process was used to produce nanosized Cu/SiC composite particles. The powders were characterized by means of chemical analysis, energy dispersive X-ray spectroscopy (EDX), transmission electron microscopy (TEM), specific surface measurements (BET), X-ray powder diffractometry (XRD) and X-ray photoelectron spectroscopy (XPS). X-ray absorption fine structure analysis (EXAFS) was performed to determine the near range order structure of the nanosized particles.

1. Introduction

Nanosized particles, i.e. particles with sizes below about 100 nm, are of growing interest for materials science and industrial applications due to their promising mechanical, chemical and electrical properties [1]. Apart from being an interesting model system, the metal/ceramic system Cu/SiC could find applications in the field of welding electrodes and electrical contacts. Recently, Cu_2O has been discussed as a photocatalyst for water splitting under visible light irradiation [2].

Several techniques, including thermal plasma processes, for the production of nanosized particles have been developed in the past [3–5]. Besides wet chemical processes and high-energy destruction (milling, mechanical alloying), many of these processes consist of an evaporation phase, where the starting materials are vaporized, followed by a quenching phase, where rapid cooling leads to a limited growth of the nucleating particles [6]. Many of these processes deal with gases and liquids as starting materials. However, recently several authors adressed the problem of the production of ultrafine particles and coatings using solid precursors [7–9]. Solids as starting materials are available at low cost for a wide class of materials, and, since pure substances can be used, no undesirable reaction products are formed. Additionally, liquid and gaseous precursors are often toxic, flammable or explosive and thus difficult to handle. On the other hand, boiling points as well as heats of evaporation are often much higher for the solid starting materials compared to liquid and gaseous precursors, so special care has to be taken for the complete evaporation of the precursor. Furthermore, the steady transport of solid material into the plasma is not easy to perform.

In the present study, the chemical composition and the structure of Cu/SiC nanoparticles synthesized in a thermal plasma process are investigated. While energy dispersive X-ray spectroscopy (EDX), chemical analysis and X-ray photoelectron spectroscopy (XPS) are used to determine the chemical composition and the valence of the individual elements, transmission electron microscopy (TEM) and the measurement of adsorption isotherms (BET) provide information about the particle size and their specific surface. In addition to X-ray diffraction (XRD) experiments, which indicate long range order correlations, extended X-ray absorption fine structure (EXAFS) measurements are carried out. EXAFS explores the modulations in an X-ray absorption spectrum that extend from approximately 40 eV above the X-ray absorption edge up to about 1000 eV or more. EXAFS is caused by the scattering of photoelectrons emerging from the absorbing atom by neighboring atoms. Since EXAFS contains quantitative information regarding the structure of the first few co-ordination shells around the absorbing atom such as bond distances, co-ordination numbers and Debye–Waller factors [10], EXAFS was successfully applied for the investigation of nanosized materials such as clusters [11–15].

2. Experimental setup

2.1. Particle preparation

The plasma reactor consists of a radio frequency generator (frequency: 3.5 MHz, max. r.f. plate power: 35 kW), a quartz plasma torch, a quenching chamber and a filter system, as schematically depicted in Fig. 1. The inductively coupled plasma is burning in pure

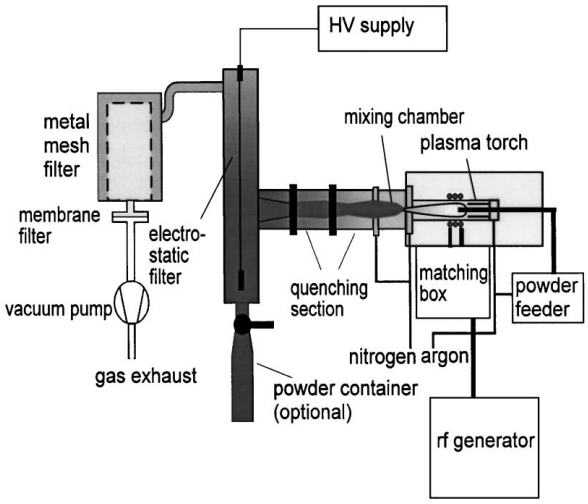

Figure 1 Schematic representation of the thermal plasma process for the production of ultrafine powders.

argon (99.999% purity) at pressure conditions of typically 400–800 hPa. Precursors can be fed both axially through the plasma and radially into the tail flame. Addition of N_2 gas (99.999% purity) in the tail flame region results in rapid quenching of the evaporated material and the formation of nanosized particles. The resulting powders are collected in a combination of an electrostatic filter and a metal mesh filter. Plasma characterization is performed by optical emission spectroscopy [16].

The r.f. generator plate power is approximately 13 kW for all experiments described here. Argon is fed into the plasma both as a sheath gas with a swirl component ($Q = 60$ slm) and axially as a central gas ($Q = 15$ slm). Copper (Aldrich, 99% purity, 10 μm maximum particle size) and silicon carbide precursor powders (Norton F600, 10 μm maximum particle size) are mechanically mixed and fed axially into the plasma through a water-cooled stainless steel injection probe by means of a powder feeder with 5 slm argon as a carrier gas. Spectroscopic measurements and numerical modeling [16] both prove temperatures of approximately 10 000 K in the hot plasma zone. This temperature is sufficient for the complete evaporation of copper powders up to a particle size of 15 μm for the present plasma conditions according to model calculations [16]. Nitrogen gas is injected as a quenching gas at two process positions: into a mixing chamber, where the gas jet is confined, and at the entrance of the quenching section (see Fig. 1). Two series of experiments are conducted: First the influence of process parameters (r.f. power, quench gas rate, powder feed rate) on the resulting powders is studied. While these first experimental runs are performed with a 50 mol % SiC precursor mixture, the second series is carried out with fixed process conditions but with different SiC contents of the precursor mixture (50, 20, 10, 5 and 0 mol % SiC). In contrast to other preparation techniques for nanosized particles (such as low pressure plasma techniques), which have production rates in the range of mg h^{-1} in the experiments described above production rates are up to 60 g h^{-1} in these experiments.

2.2. Particle characterization

The content of C, N and O in the powders has been determined by standard methods: IR spectroscopy after combustion in an oxygen flow (LECO method, carbon), and hot extraction in a He gas flow with subsequent heat conductivity detection and IR spectroscopy, respectively (N, O).

Transmission electron micrographs are recorded with a Philips EM 400 T microscope. Powder samples are suspended in water (1 mg ml^{-1}), ultrasonically deagglomerated, diluted (1:100) and prepared on a copper mesh coated with a thin formvar film. Magnifications up to 100 000 are used to determine size and morphology of the particles.

EDX measurements are carried out on an ISI-60 (International Scientific Instruments) scanning electron microscope using 30 keV electron energy. The characteristic X-ray emission is measured by a Si(Li) detector. The energy resolution in the multichannel analyzer is approximately 160 eV (for the MnK_α line). Due to the low energy limit of detection (<1 keV), light elements, such as carbon and oxygen are not detectable with this equipment.

Diffractograms were measured in the Bragg–Brentano focusing geometry using a Siemens D 5000 powder diffractometer in the range of $2\theta = 20°$–$75°$ at a scanning speed of 0.06° min^{-1} with CuK_α radiation.

XPS experiments are performed with a commercial spectrometer (ESCALAB 200X, Fisons/VG Scientific) equipped with a spherical sector analyzer (VG Scientific MKII). XPS spectra are obtained with non-monochromatized MgK_α- and AlK_α-radiation ($h\nu$ = 1253.6 eV and 1486.6 eV, respectively) with an input power of 300 W (15 kV, 20 mA); all photoelectron spectra are taken in the constant analyzer energy (CAE) mode with a pass energy of 20 eV. The calibration of the spectrometer is routinely checked with sputter cleaned Au, Ag and Cu specimens according to [17]. Under routine operating conditions, the vacuum in the analyzer is better than 5×10^{-7} Pa. The powder specimens are mounted on specimen stubs with a conducting tape and introduced to the UHV-system of the spectrometer via a fast entry air lock. Since the samples are partially isolating, the C 1s peak is used as an additional internal reference for binding energy calibration.

The EXAFS data are collected in the vicinity of the CuK edge (8.98 keV) using a double crystal monochromator with two flat Si (1 1 1) crystals. The crystals can be detuned with respect to each other using a piezo-crystal to reduce the amount of harmonics in the Bragg-reflected beam [18]. The experiments are performed at the RÖMO II beamline (bending magnet station) [19] at the DORIS III storage ring at HASYLAB (Hamburg, Germany) operating with ≈70–100 mA of stored 4.4 GeV positron current. Conventional transmission mode EXAFS spectra are recorded within about 15 min. Incident and transmitted intensities are measured by means of argon filled ionization chambers. A copper metal foil, crystalline Cu_2O, CuO and $CuCO_3$ powders pressed in polyethylene are measured in transmission to obtain standard spectra.

TABLE I Results of chemical analysis of Cu/SiC nanoparticles produced in a thermal r.f. plasma process. C_{th} is the carbon weight fraction calculated from the SiC content of the precursor powder mixture (given for comparison)

SiC content precursor powder (mol %)	C (%)	C_{th} (%)	N (%)	O (%)
50	11.7	11.6	1.69	9.9
20	3.8	4.1	1.08	7.7
10	1.78	2.0	0.81	10.4
5	1.1	0.95	0.32	7.0
0	0.40	0	0.06	11.5

3. Results and discussion

Samples of the produced powders were characterized concerning their chemical composition, particle size, crystal structure and their electronic situation. The results of chemical analysis are compiled in Table I. Independent of the Cu/SiC ratio, all samples show a high oxygen content of about 10 mass %, which is attributed to air contact of the powders after preparation. The powders are pyrophoric when exposed to air, which is typical for metal-containing nanosized powders [20]. Additionally, up to 2 mass % nitrogen was detected in the powder. The amount of nitrogen found in the samples increases with higher SiC content, indicating that nitrogen is predominantly bound (physically or chemically) to SiC. The amount of carbon measured for the ultrafine samples is in agreement with the values calculated from the SiC content of the precursor powders.

Transmission electron microscopy is performed for several samples to determine the particle size. Micrographs and measured particle size distributions for different quench gas flow rates (N_2, mixing chamber) are presented in Fig. 2. In both cases, a powder feed rate of 12 g h^{-1} and an r.f. plate power of 12 kW is applied. The micrographs show agglomerated particles. Since Cu can be distinguished from SiC due to its higher contrast, a composite character of the powders on a nm-scale can be seen. While the average particle size is about 10 nm for the individual particles, the mean diameter of the Cu core is significantly smaller with values of approximately 5–6 nm. The reduction of the quenching gas rate (quench gas flow introduced into the mixing chamber is omitted) results in a higher mean particle size (25 nm compared to 10 nm) as can be seen in Fig. 2b due to an increased growth time for the particles. The resulting particle size distributions are presented in Fig. 3a for both situations. Such a decrease of the average particle size was already observed in several

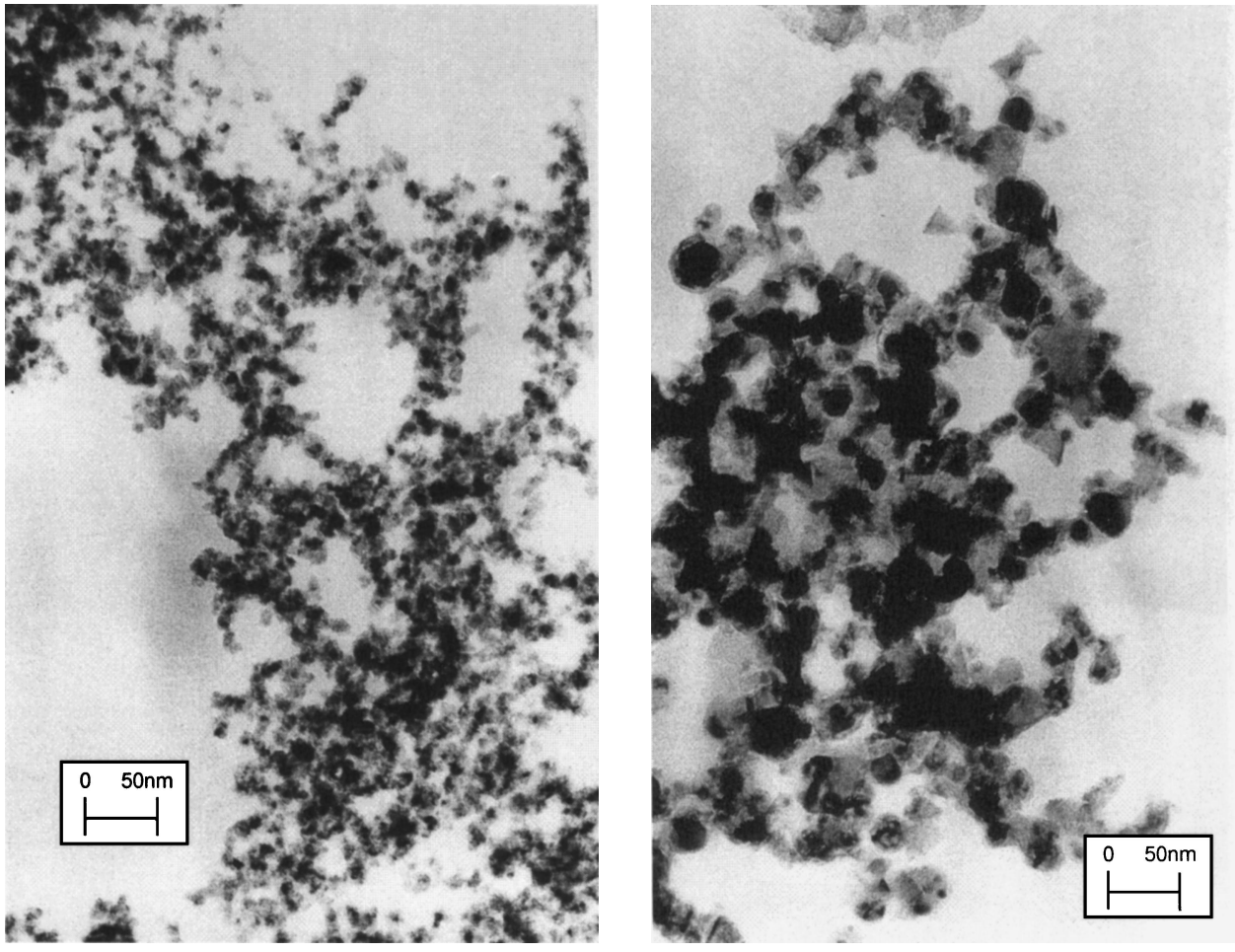

(a) (b)

Figure 2 (a) Transmission electron micrograph of Cu/SiC particles synthesized in a thermal plasma (12 g h^{-1} powder feed rate, 12 kW r.f. plate power) and quenched with a high quenching rate in the mixing chamber (60 slm), and (b) transmission electron micrograph of Cu/SiC particles synthesized in a thermal plasma (12 g h^{-1} powder feed rate, 12 kW r.f. plate power) and quenched with a low quenching rate (0 slm, no additional nitrogen gas in the mixing chamber).

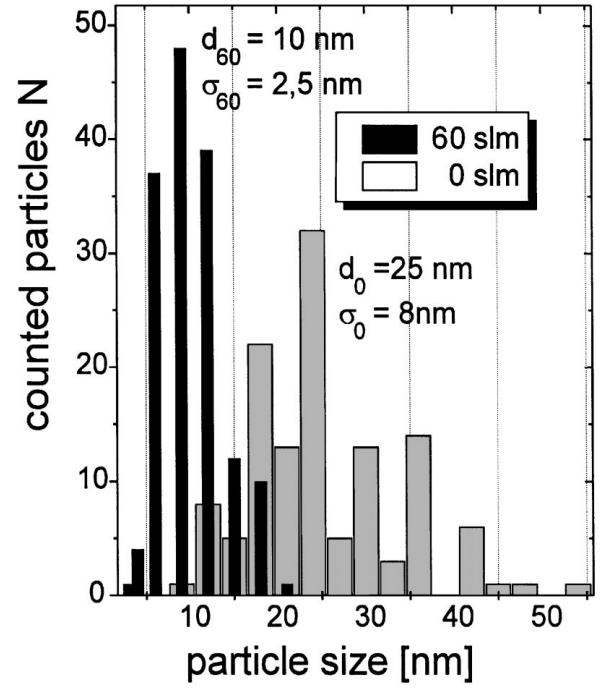

(a)

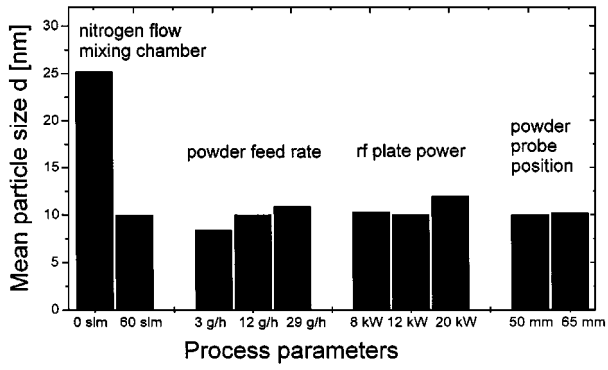

(b)

Figure 3 (a) Measured particle size distributions determined from transmission electron micrographs for 12 g h^{-1} powder feed rate and 12 kW r.f. plate power and two different quenching gas rates (d: mean particle size, σ: standard deviation), and (b) mean particle size for different process conditions.

particle systems by other authors (e.g. [6, 21]). Corresponding values for the specific surface area of the powder samples determined by the BET method are 115 m^2 g^{-1} and 200 m^2 g^{-1} for the low and the high quenching rate, respectively. Variation of single process parameters other than the quenching rate (starting from standard conditions of 12 kW r.f. power, 60 slm quench gas rate, 12 g h^{-1} feed rate and 50 mm powder probe position) have only minor effect on the particle size as can be seen from Fig. 3b, in which the mean particle size is shown for several experimental conditions. For example, only a slight increase in particle size from about 8 nm for 3 g h^{-1} powder feed rate to approximately 11 nm for 29 g h^{-1} powder feed rate can be seen, while an increased r.f. plate power does not systematically influence the particle size.

Scanning electron microscopy in combination with energy dispersive X-ray spectroscopy (EDX) was used to determine the atomic composition of the samples on a microscopic scale. X-ray spectra of the precursor powders and of ultrafine powder samples were recorded. Since the EDX signal originates from an area of approx. 1 μm $\times$ 1 μm, the spectra of the precursor particles (approximately 10 μm diameter) show nearly pure Cu and Si peaks, respectively, while in the ultrafine composite powders both Si and Cu peaks can be seen. This is a further indication of a composite character of the particles. The intensity relation between Si and Cu peaks follows the Si/Cu ratio in the precursor powder mixtures similar to the results of chemical analysis (Table I).

Diffractograms of the powder samples of different SiC-content are shown in Fig. 4. While the observed peak broadening of the detected Bragg peaks can be related to the nm-size of the individual crystallites, the increasing background intensity for smaller Bragg angles indicates that at least a fraction of the investigated material is in an amorphous state. Due to air contact of the powders, additionally to SiC and Cu peaks intense copper oxide peaks can be seen (CuO for one sample, Cu_2O for the other samples).

No crystalline Si, SiO_2 or Si_3N_4 can be found in the diffractograms, indicating that the oxygen content of the powders is mainly caused by Cu_2O and adsorbed oxygen. The oxidic peaks are broader than the structures due to Cu and SiC indicating a smaller crystallite size for the oxidic species, which is reasonable for a surface oxide layer on a metallic particle core (see also the results of X-ray photoelectron spectroscopy below).

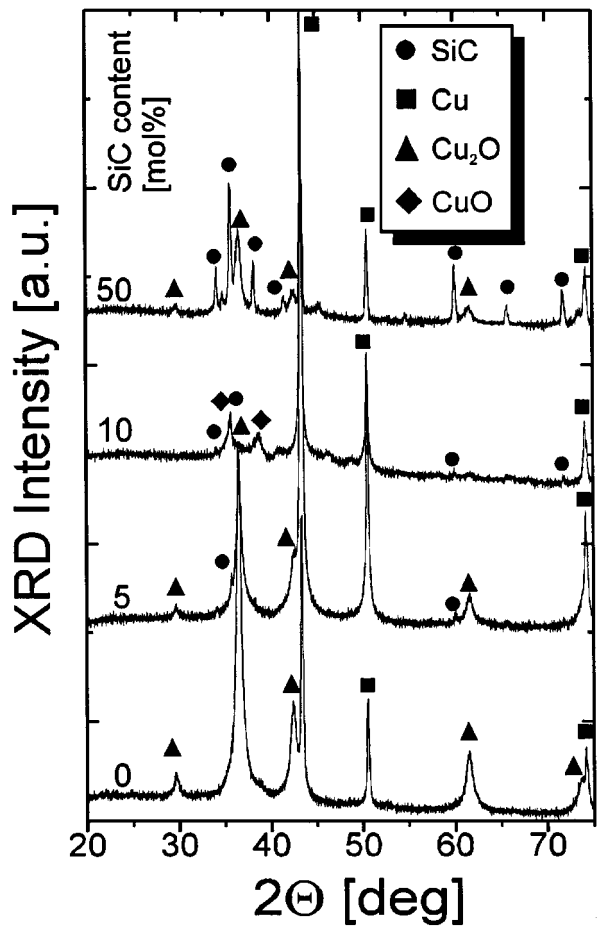

Figure 4 Powder diffractograms of nanosized Cu/SiC-particles with different SiC-content. Bragg peaks related to SiC (●), metallic Cu (■), Cu_2O (◆) and CuO (▲) are indicated.

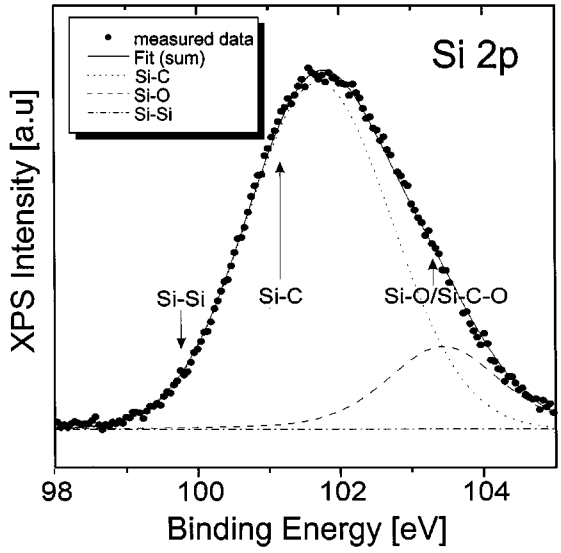

Figure 5 XPS spectrum of nano-Cu/O/SiC with 50 mol % SiC, Si 2p peak. Measured data and fitted results, peak energies of several Si-compounds are indicated.

In general, X-ray photoelectron spectroscopy (XPS) is a surface sensitive technique due to a photoelectron mean free path length of 2–3 nm. For the ultrafine powders this is a considerable part of the whole particle. In the Si 2p photoelectron spectrum in Fig. 5 no Si–Si bonds with a binding energy of E_B = 99.3 eV [22–24] can be seen. The asymmetry of the peaks at high binding energies indicates that besides Si–C, Si–O bindings are also present in the samples. A least squares fit of the spectrum in Fig. 5 using three Gauss–Lorentz functions representing Si–Si, Si–C and Si–O bindings resulted in less than 0.1% Si–Si, approximately 82% Si–C and 18% Si–O. Since no SiO_2 was found in the diffractograms, either crystalline SiO_2 forms an extremely thin layer on the surfaces of the particles or amorphous Si–O structures are dominant. The Cu $2p_{3/2}$ photoelectron spectra and X-ray induced Cu LMM Auger spectra prove the presence of Cu(I) oxide species at the surface of the powders when compared to Cu (metallic), Cu(I) and Cu(II) reference compounds (see, e.g. [25]). Therefore, the powders very probably consist of a metallic Cu core and Cu_2O (see Fig. 6).

X-ray absorption fine structure spectra obtained above the CuK-edge of several Cu/SiC nanoparticles with 50 mol % SiC, the Cu/SiC precursor material and some Cu reference compounds are displayed in Fig. 7a. The near edge region (XANES) of these spectra is displayed in the insert. Obviously, the XANES measured for the Cu/SiC precursor material is very different from the nanosized powders. These spectra reveal intense white line features at about 9000 eV which are typical of Cu_2O and CuO (see insert of Fig. 7a). However, neither the Cu_2O nor the CuO reference spectrum agree satisfactorily with those of the nanosized particles. For example, the pre-edge feature of Cu_2O at about 8980 eV as well as a characteristic CuO structure at about 9015 eV are not present for the nanoparticles. For further data evaluation, the photon energy was converted to a wave number scale. After subtraction of a smooth background, the absorption fine structure data $\chi(k)$ were determined for each spectrum and the k^3-weighted fine structure $\chi(k)^*k^3$ were Fourier-transformed (FT). In Fig. 7b, the magnitude of the FT ($\chi(k)^*k^3$) is shown for the X-ray absorption data of Fig. 7a. The FTs are dominated by the short range order structure of the samples, i.e. peaks in these FTs correspond to the first few co-ordination shells in the vicinity of the absorbing Cu atom. Owing to the photoelectron phase shift arising from the scattering processes, all peaks in the FTs are generally shifted towards lower distances compared to their real crystallographic distances (see, e.g. [10]). For example, the peak at a radial distance of about 0.15 nm in the FT of Cu_2O (cuprit) can be related to two oxygen nearest neighbors with a radial distance $R = 0.185$ nm and the peak at approximately 0.23 nm in the FT of the precursor powder corresponds to a Cu–Cu bond in f.c.c. copper at a distance of $R = 0.252$ nm with 12 nearest neighbors. It should be noted that this FT is very similar to that of a copper metal foil, while contributions of Cu_2O/CuO and metallic Cu are visible in the FTs of the nanosized powders; i.e. the nanoparticles seem to be a

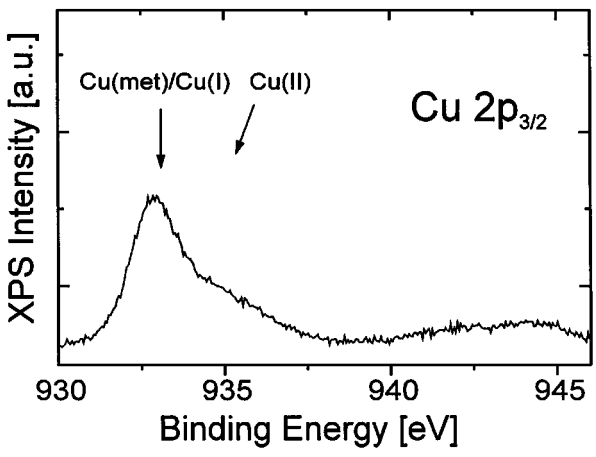

(a)

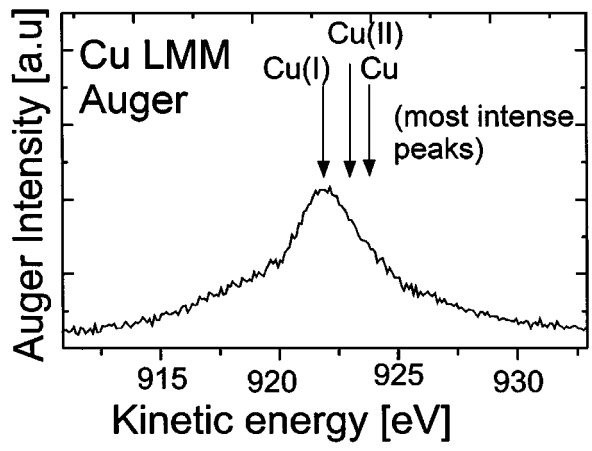

(b)

Figure 6 (a) XPS spectrum, Cu $2p_{3/2}$ peak of a nanosized Cu/SiC powder with 50 mol % SiC, and (b) X-ray irradiated Auger electron spectrum of a 50% SiC/Cu sample, Cu LMM peak.

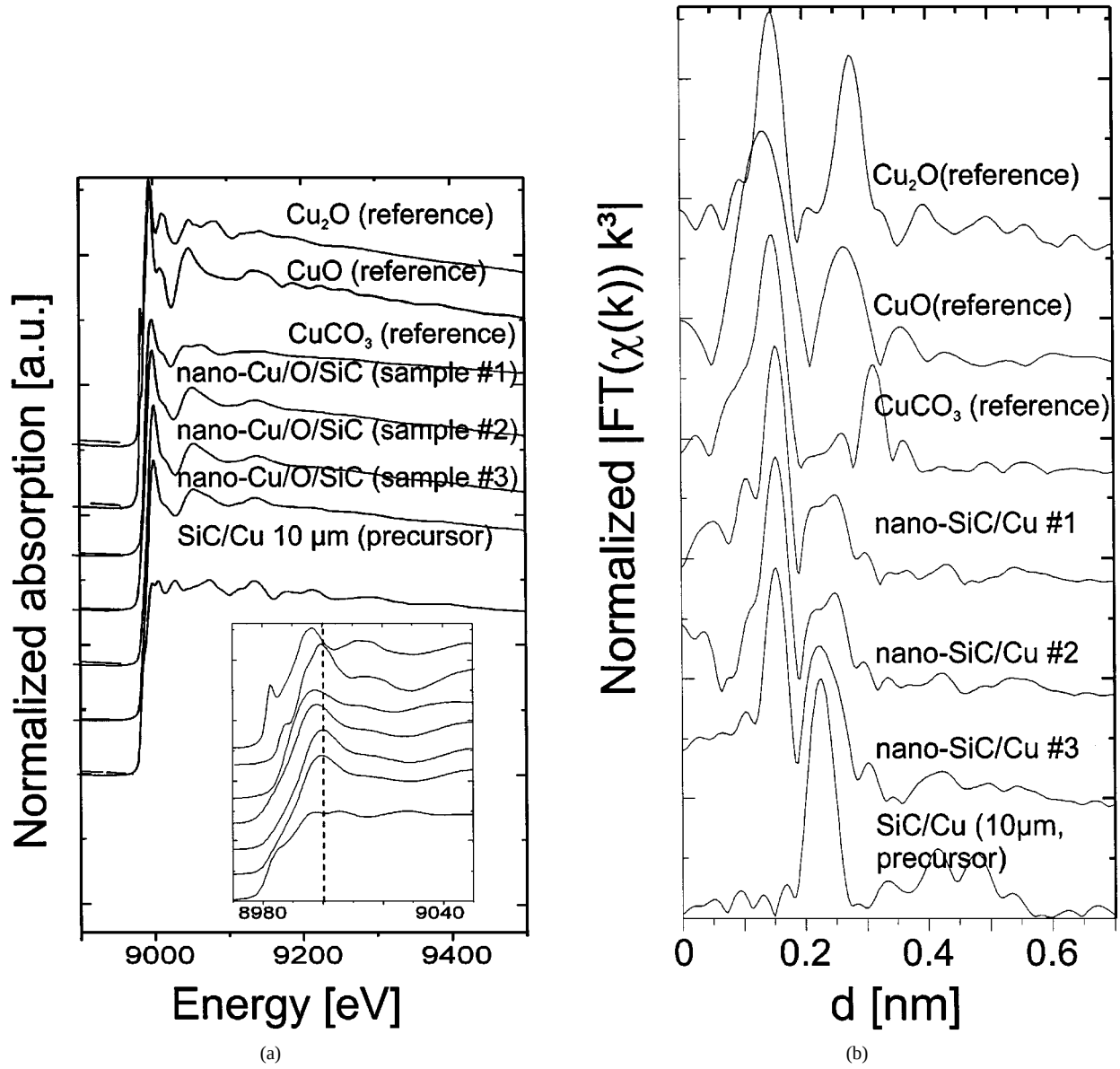

Figure 7 (a) X-ray absorption spectra of several nanosized Cu/SiC powders, the Cu/SiC precursor material and several reference compounds obtained above the CuK edge at 8979 eV. The insert depicts the near edge region of all spectra in more detail, and (b) magnitude of the Fourier-transform (FT) of the k^3-weighted EXAFS structures presented in Fig. 7a.

mixture of metallic Cu, Cu_2O and CuO. From the results presented it is obvious that $CuCO_3$ is not present in the nanoparticles since the intense $CuCO_3$ coordination at about 0.31 nm is absent in the FTs of the nanoparticles.

Compared to the spectra of the reference compounds, however, it seems as if the second (Cu–Cu) co-ordination of the oxides at about 0.27 nm (Cu_2O) and 0.25 nm (CuO) are less developed for the nanoparticles. It can therefore be assumed that the near range order structure of the oxidic component is highly disordered compared to the crystalline Cu-oxide reference compounds.

For a more detailed analysis of the atomic short range order structure of the nanoparticles, the first Cu–O co-ordination shell ($0.08\,\text{nm} \leq d \leq 0.19\,\text{nm}$) was isolated by means of a filter function and back-transformed into k-space. These back-transformed data were fitted with a single shell model, i.e. a Cu–O co-ordination shell, with calculated phases and amplitudes [26]. Fit results for the interatomic distance R, the co-ordination number N and the disorder parameter σ (mean square displacement) are compiled in Table II for several Cu/SiC nanoparticle samples, crystalline Cu_2O and CuO. Obviously, the Cu–O binding radius $R \approx 0.193 \pm 0.001$ nm is larger for the nanoparticles when compared to Cu_2O ($R = 0.185$ nm in agreement with literature data [27]) but smaller than for CuO ($R = 0.195$ nm). However, the average number of nearest neighbors $N \approx 2.5 \pm 0.25$ is significantly smaller than expected for CuO ($N = 4$, [27]). Compared to crystalline CuO, the obtained disorder is slightly enhanced, indicating a higher degree of disorder even in the first co-ordination shell. In summary, the results of the EXAFS investigations suggest that an appreciable part of the plasma synthesized Cu/SiC nanoparticles consist of Cu oxides, which can be described as a mixture of Cu_2O and CuO, and a smaller fraction of metallic copper.

TABLE II Fit results for the first Cu–O co-ordination shell of several nanosized Cu/SiC powders with 50 mol % SiC. (Values in brackets: crystallographic data for CuO and Cu_2O from [27])

	Nano-Cu/O/SiC (sample #1)	Nano- Cu/O/SiC (sample #2)	Nano-Cu/O/SiC (sample #3)	Cu_2O (reference)	CuO (reference)
R (nm)	0.1944	0.1932	0.1922	0.1850 (0.185)	0.1951 (0.188/0.196)
N	3.0	2.3	2.2	1.9 (2)	3.4 (2+2)
σ (nm)	0.0079	0.0073	0.0076	0.0072	0.0064

4. Summary and conclusions

A thermal induction plasma reactor was built to produce ultrafine Cu/SiC/O composite particles. TEM micrographs show an average particle size of 10 to 25 nm, depending on the quench gas rate. The composite character of the particles is visible via the different electron density of Cu and Si in the TEM micrographs and—on a 1 μm scale—by EDX. Diffractometry reveals partially amorphous, partially crystalline structures. Copper oxide peaks can be seen when powders are exposed to air, while crystalline SiO_2 is not detectable. XPS spectra indicate that at the surface of the nanopowders Si is bound as Si–C and Si–O. The copper fraction of the nanosized particles consists of an oxidic surface and a metallic copper core as shown by X-ray diffraction and XPS.

EXAFS investigations at the CuK-edge reveal a more disordered near range order structure of the oxidic components of the particles. This finding agrees qualitatively with the observed amorphous background in the XRD experiments.

Acknowledgements

The authors wish to thank Professor Dr V. Kolb-Bachofen, Mrs M. Lenzen, and Dr H. Hammer (all University Düsseldorf) for performing TEM and EDX measurements. Furthermore, thanks to Dr J. Viets (University Dortmund), Mr M. Michulitz and Mr P. Lersch (Forschungszentrum Jülich) for carrying out BET measurements, chemical analysis and most of the XRD measurements. Special thanks to Dr R. Vaßen (Forschungszentrum Jülich) for supporting the powder characterization.

References

1. R. SIEGEL, "Nanophase Materials," in "Encyclopedia of Applied Physics," **11** (1994) p.173.
2. M. HARA, T. KONDO, M. KOMODA, S. IKEDA, K. SHINOHARA, A. TANAKA, J. N. KONDO and K. DOMEN, *Chem. Commun*. **3** (1998) 357.
3. R. M. YOUNG and E. PFENDER, *Plasma Chem. Plasma Process* **5** (1985) 1.
4. P. C. KONG and Y. C. LAU, *Pure Appl. Chem*. **62** (1990) 1809.
5. R. A. ANDRIEVSKI, *J. Mater. Sci*. **29** (1994) 614.
6. T. YOSHIDA, *Mater. Trans. JIM* **31** (1990) 1.
7. K. TERASHIMA, H. KOMAKI and T. YOSHIDA, *IEEE Trans. Plasma Sci*. **18** (1990) 980.
8. J. Y. GUO, F. GITZHOFER and M. I. BOULOS, *J. Mater. Sci*. **30** (1995) 5589.
9. B. MICHELT, G. LINS and R. J. SEEBÖCK, *Proc. ISPC* **12** (1995) 1993.
10. D. C. KONINGSBERGER and R. PRINS, "X-ray absorption: Principles, Applications, Techniques of EXAFS, SEXAFS and XANES," (Wiley, New York, 1988).
11. T. YOKOYAMA, S. KIMOTO and T. OHTA, *Jpn. J. Appl. Phys*. **28** (1989) L851.
12. M. A. MARCUS, W. FLOOD and M. STIEGERWALD, *J. Phys. Chem*. **95** (1991) 1571.
13. C. PAK, S. J. CHO and J. Y. LEE, *J. Catal*. **149** (1994) 61.
14. S. KAKAR, O. BJÖRNEHOLM, J. WEIGELT, A. R. B. DE CASTRO, L. TRÖGER, R. FRAHM and T. MÖLLER, *Phys. Rev. Lett*. **78** (1997) 1675.
15. F. CIMINI and R. PRINS, *J. Phys. Chem. B* **101** (1997) 27.
16. P. BUCHNER, H. FERFERS, H. SCHUBERT and J. UHLENBUSCH, *Plasma Sources Sci. Technol*. **6** (1997) 450.
17. M. T. ANTHONY and M. P. SEAH, *Surf. Interface Anal*. **6** (1984) 95.
18. G. MATERLIK and V. O. KOSTROUN, *Rev. Sci. Instrum*. **51** (1980) 86.
19. R. FRAHM, *ibid*. **60** (1989) 2515.
20. R. M. YOUNG and E. PFENDER, *Plasma Chem. Plasma Process* **5** (1985) 1.
21. R. MACH, H.-D. KLOTZ, K.-D. SUHRKE, H. DROST, F. OLESZAK, G. LACAYO and K. SZULZEWSKI, *Proc. ISPC* **11** (1993) 53.
22. R. NORDBERG, H. BRECHT, R. G. ALBRIDGE, A. FAHLMAN and J. R. VAN WAZER, *Inorg. Chem*. **9** (1970) 2469.
23. W. MORGAN and J. R. VAN WAZER, *J. Phys. Chem*. **77** (1973) 964.
24. R. C. GRAY, J. C. CARVER and D. M. HERCULES, *J. Electron Spectrosc. Relat. Phenom.* **8** (1976) 343.
25. P. DRUSKA and H.-H. STREHBLOW, *Surf. Int. Anal*. **23** (1995) 440.
26. J. J. REHR, R. C. ALBERS and S. I. ZABINSKY, *Phys. Rev. Lett*. **69** (1992) 3397.
27. R. W. G. WYCKOFF, "Crystal structures" Vol. 1, 2nd Edn., (Interscience Publishers, New York, 1963).

Received 30 June
and accepted 30 July 1998